

Supporting Information: Ultrafast Ring Closing of a Diarylethene-Based Photoswitchable Nucleoside

Yang Li,[†] J. Luis Pérez Lustres,[†] Hans-Robert Volpp,[†] Tiago Buckup,[†] Theresa
Kolmar,[‡] Andres Jäschke,^{*,‡} and Marcus Motzkus^{*,†}

[†]*Physikalisch Chemisches Institut, Ruprecht-Karls University, D-69120 Heidelberg, Germany*

[‡]*Institut für Pharmazie und Molekulare Biotechnologie, Ruprecht-Karls University, D-69120
Heidelberg, Germany*

E-mail: jaeschke@uni-hd.de; marcus.motzkus@pci.uni-heidelberg.de

Phone: +49 (0)6221 54 8727. Fax: +49 (0)6221 54 8720

a) fs Transient Absorption Setup

A previous version of the fs transient absorption setup was described elsewhere.¹ The system was recently upgraded so that a thorough description is pertinent.

Fundamental pulses are derived from a Ti:Sa regenerative amplified laser system (CPA 1000, Clark MXR, Inc.). The laser delivers 650 μJ , 150 fs pulses at 1 kHz. The output is split for white-light continuum generation (30 μJ) and optical pumping in the UV.

The UV pump is obtained by sum frequency generation of the fundamental (140 μJ) and the compressed output (15 μJ , 25 fs) of a home-built two-stage non-collinear optical parametric amplifier (NOPA) tuned to 530 nm.² The NOPA output is compressed with a fused-silica prism pair and focused onto a 90 μm thick BBO crystal ($\theta = 40.5^\circ$) for sum frequency generation with 800 nm,

150 fs pulses. The so-obtained UV pulses ($1 \mu\text{J}$, 40 fs) were not further compressed. They are centred at typically 325 nm and have a spectral width of 9 nm. The pulse duration is estimated by two-photon autocorrelation³ and is about 40 fs, Figure SI 1.

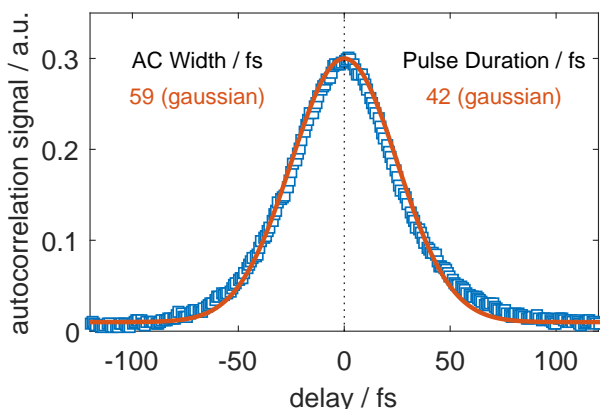


Figure SI 1: Typical two-photon autocorrelation of the excitation pulse centered at 327 nm (blue squares). The autocorrelation was fitted to a gaussian function, orange solid line. The full-width at half maximum of the autocorrelation function and the pulse duration are indicated in the inset.

The continuum is used as broadband optical probe from the near-UV to the Vis. It is generated by focusing ($f = +50 \text{ mm}$, $NA = 0.1$) the fundamental laser beam onto a 5 mm CaF_2 plate, which is oriented and continuously shifted in perpendicular directions. The continuum is parallelized with a parabolic mirror, steered with UV-enhanced aluminum mirrors and focused onto the flowing sample cell (Starna 48/UTWA/Q/0.2, with 0.2 mm thick windows and 0.2 mm path-length). The transmitted light is parallelized with a lens, filtered, dispersed with a fused-silica prism and focused onto a photodiode array with 256 elements (Hamamatsu 3904-256Q). The spectrograph is calibrated with a set of 25 narrow-pass filters (Andover Corporation). Transient absorption is calculated from consecutive pump-on and pump-off measurements and averaged over 1000 shots. A data set results from the average of eight independent scans. Measurements were performed with parallel and perpendicular polarizations at constant step sizes.

Transient spectra were corrected for the chirp of the white-light continuum with the help of the non resonant coherent solvent signal.⁴ The latter was fitted with a time-dependent Gaussian func-

tion and its first four time derivatives, see Figure SI 2. The fit delivers the wavelength dependent instrument response function (Figure SI 3) and the time-zero function (Figure SI 4).

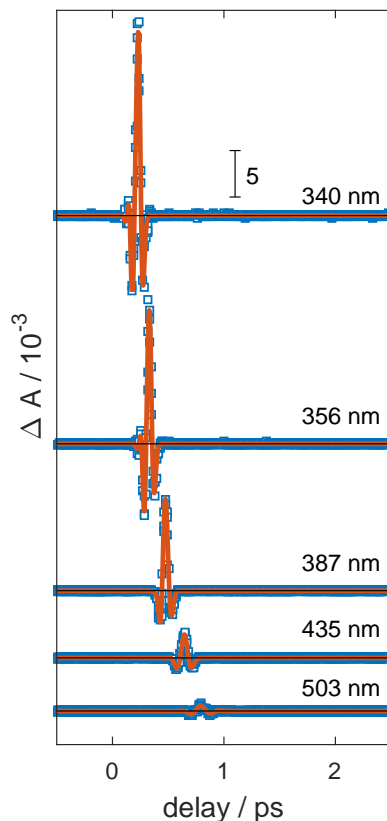


Figure SI 2: Non resonant solvent signal (methanol, blue squares) measured with 327 nm excitation at the indicated probe wavelengths. The signal was fitted with a Gaussian function and its first four time derivatives (red lines). The time-zero function and the wavelength-dependent pump-probe cross-correlation are estimated from these fits.

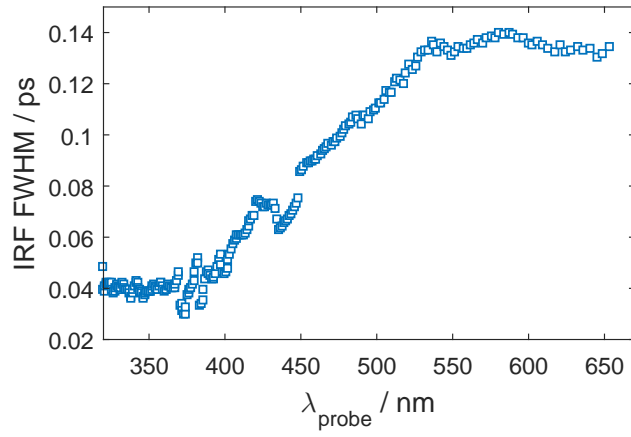


Figure SI 3: Wavelength-dependent pump-probe cross-correlation estimated by the fits shown in Figure SI2.

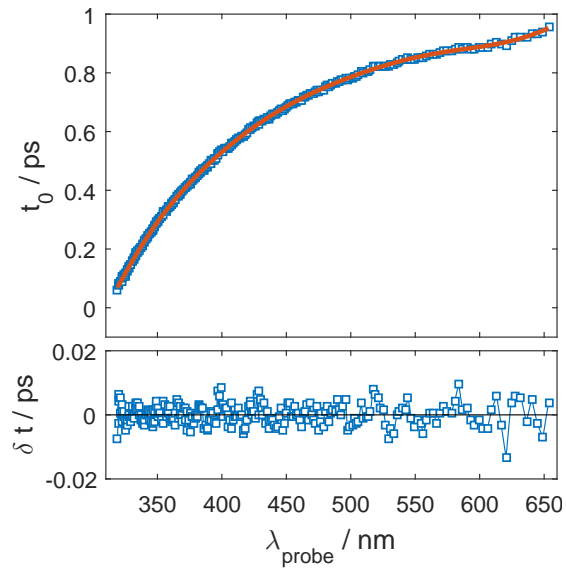


Figure SI 4: Time-zero function (blue squares) resulting from the fits shown in Figure SI2. The final time zero function was obtained by fitting a tenth order polynomial to the data (red solid line). The lower panel shows the residuals of the time zero function.

b) H-NMR Spectrum of PS-IV in deuterated Chloroform and determination of the quantum yield of the ring closing reaction

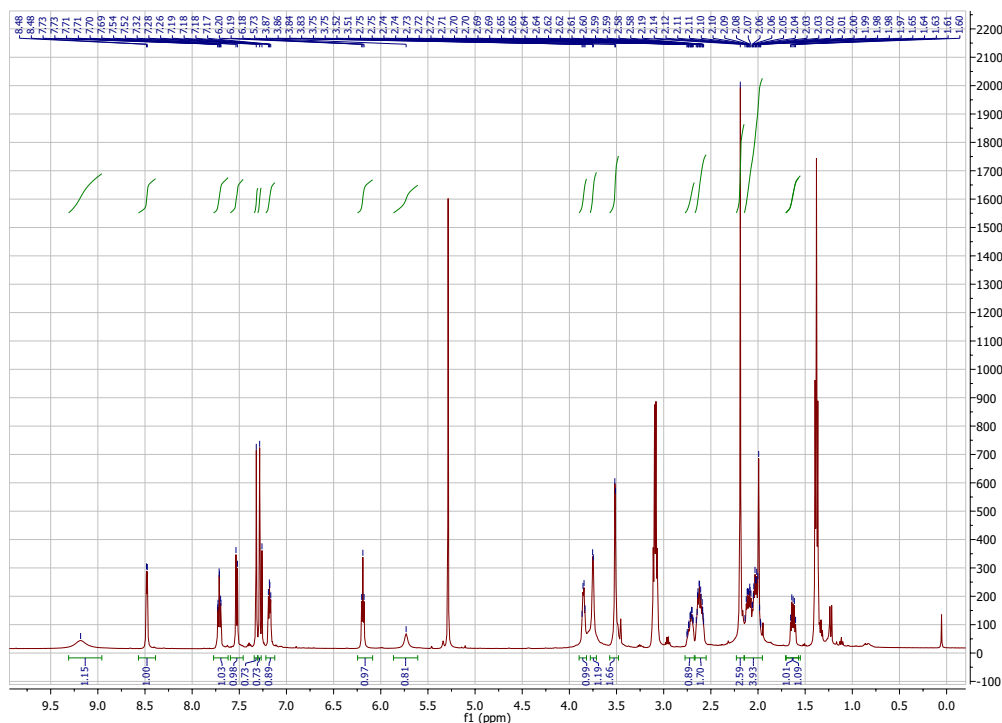


Figure SI 5: 500 MHz H-NMR Spectrum of PS-IV in deuterated chloroform. δ (in ppm) = 9.18 (s, 1H), 8.48 (d, 1H), 7.71 (dt, $J = 5, 5$ Hz, 1H), 7.53 (d, $J = 10$ Hz, 1H), 7.32 (s, 1H), 7.28 (s, 1H), 7.18 (dt, $J = 5, 5$ Hz, 1H), 6.19 (t, $J = 5, 5$ Hz, 1H), 5.73 (s, 1H), 3.84 (q, $J = 5$ Hz, 1H), 3.75 (d, 1H), 3.51 (d, 2H), 2.75-2.69 (m, 1H), 2.65-2.58 (m, 2H), 2.19 (s, 3H), 2.14-2.07 (m, 4H), 1.65-1.60 (m, 1H).

In the open form of diarylethenes two different conformers exist: the parallel and the antiparallel conformations. Only the antiparallel conformation is able to convert to the closed form upon UV-Irradiation. For symmetric diarylethenes the ratio between the two conformers is about 1:1 as shown by NMR spectroscopy.⁵ Usually, symmetric diarylethenes bear one methyl group on each aryl ring. The methyl groups show different NMR-signals in the parallel and antiparallel conformations. Consequently, the NMR-spectrum of the corresponding diarylethenes displays a doublet for the Methyl-H signal. By integrating the peaks, the ratio of the two conformers is calculated. In contrast, the H-NMR spectrum in Figure SI 5 shows a single sharp H-methyl peak centred at

2.19 ppm, from which a major contribution of the antiparallel conformation is deduced.

The calculation of the quantum yield for the ring closing reaction followed the procedure outlined by Jong et al. in Reference 6. Basically, a solution of the O isomer was irradiated with light of 285, 304 and 330 nm for a short period of time (2-5 seconds, depending on the irradiation wavelength). The beams were derived from a parametric amplifier (TOPAS Prime, Light Conversion). A typical power of 200 mW was used. The irradiation time was kept short enough to neglect changes in the absorption of the O isomer (less than 10%). The beam was expanded to a diameter of about 6 cm, so that homogeneous irradiation of the cell can be assumed. The stationary UV-Vis absorption was measured afterwards. The latter reflects the absorption changes induced by irradiation since the thermal back reaction is very slow in the ground state. The number of absorbed photons is estimated by measuring the fluence, the cell cross-section and the absorption of the O isomer at the irradiation wavelength. The number of molecules produced photochemically as C isomers is measured through the absorption coefficients calculated in the next section. The ratio between the number of C molecules and the number of absorbed photons provides an estimate of the reaction quantum yield.

c) Method of the determination of the UV–Vis absorption spectrum of the C form by analysis of photostationary state at various irradiation wavelengths

Light irradiation shifts the ground state $O \rightleftharpoons C$ equilibrium, where O and C stand for the open and closed forms, respectively. The ground-state concentrations evolve continuously as consequence of photoconversion until the photostationary (PS) state is reached. In the latter, the C and O forms inter-convert at the same rate, so that no net change is further observed. The condition of PS state is stated in Equation SI.1. Note that the concentrations remain constant in darkness because the thermal processes show high activation energies. This enables the determination of the absorption spectrum for any given irradiation time.

$$\frac{d[O]}{dt} = \frac{d[C]}{dt} = 0 \quad (\text{SI.1})$$

The quantum yield for photoinduced conversion from the O form to the C form (ring closing) is Φ_{rc}^λ . Conversely, the quantum yield of the reverse process (ring opening) is Φ_{ro}^λ . In view of the changes observed in the absorption spectrum upon irradiation, no other photoproducts need to be considered. Under these assumptions, one deduces the following relationship for the photostationary state in the limit of low absorption. $I_0(\lambda)$ is the incident light intensity at the irradiation wavelength λ and ε_i^λ are the absorption coefficients of the closed ($i = C$) and open ($i = O$) forms at the irradiation wavelength and ℓ is the optical pathlength.

$$\left(\frac{d[O]}{dt} \right)_{PS} \approx -2.303 \times I_0(\lambda) \varepsilon_O^\lambda \ell [O] \Phi_{rc}^\lambda + 2.303 \times I_0(\lambda) \varepsilon_C^\lambda \ell [C] \Phi_{ro}^\lambda = 0 \quad (\text{SI.2})$$

$$\left(\frac{[C]}{[O]}\right)_{PS} \approx \frac{\varepsilon_O^\lambda}{\varepsilon_C^\lambda} \times \frac{\Phi_{rc}^\lambda}{\Phi_{ro}^\lambda} \quad (\text{SI.3})$$

Thus, the photostationary concentrations of the O and C forms mirror, in the low absorption limit, the relative quantum yield of photoconversion weighted by the absorption coefficients of both forms. Therefore, one can easily see that irradiation at an isosbestic point leads to a photostationary state depending solely on the quantum yields of the direct and reverse photoconversions. Equation SI.3 also shows that the full population can be converted from C to O if irradiation is accomplished at wavelengths where only C absorbs. In turn, conversion from O to C cannot be complete because the UV–Vis absorption spectrum of O overlaps the spectrum of C, so that no wavelength is available where only O absorbs. In general, irradiation in the UV will lead to a PS state containing various contributions of the C and O forms. Consequently, the absorption spectrum of the O form is experimentally known but that of C can not be easily isolated by experimental means. We discuss in the following a strategy to estimate the absorption spectrum of the C form by inspection of PS states obtained at various irradiation wavelengths.

The UV–Vis absorption spectrum at any time t in the irradiation experiment can be described as a linear superposition of the absorption spectra of the O and C forms, Equation SI.4.

$$A(t) = \varepsilon_O^\lambda \ell [O](t) + \varepsilon_C^\lambda \ell [C](t) \quad (\text{SI.4})$$

The time-dependent mole fraction of the O form in the irradiation experiment is defined as $\chi(t)$. Equation SI.4 can be now rewritten as

$$A(t) = \varepsilon_O^\lambda \ell \chi(t) c_0 + \varepsilon_C^\lambda \ell [1 - \chi(t)] c_0 \quad (\text{SI.5})$$

which divided by the experimentally known total concentration c_0 and the cell length ℓ yields

$$\epsilon(t) = \varepsilon_O^\lambda \chi(t) + \varepsilon_C^\lambda [1 - \chi(t)] \quad (\text{SI.6})$$

We express Equation SI.6 in matrix form with the help of some definitions, Equation SI.7. The species-associated-spectra matrix \mathbb{S} contains the absorption coefficients of the O and C forms in columns. $\mathbb{X}(t)$ is a column vector which contains the mole fractions of the O and C forms at time t .

$$\varepsilon(t) = \mathbb{S} \times \mathbb{X}(t) \quad (\text{SI.7})$$

Alternatively, singular value decomposition describes every spectrum in the series $\varepsilon(t)$ as a linear combination of the principal eigenvectors. The equation can be written in matrix form as Equation SI.8, where \mathbb{C} is a column vector, whose components multiply the eigenvectors in \mathbb{V} .

$$\varepsilon(t) = \mathbb{V} \times \mathbb{C}(t) \quad (\text{SI.8})$$

It is now possible to define a 2-by-2 transformation matrix \mathbb{T}^{-1} which converts \mathbb{V} into \mathbb{S} by multiplication from the right. The following relation holds.

$$\underbrace{\mathbb{V} \times \mathbb{T}^{-1}}_{\mathbb{S}} \times \underbrace{\mathbb{T} \times \mathbb{C}(t)}_{\mathbb{X}(t)} = \mathbb{S} \times \mathbb{X}(t) \quad (\text{SI.9})$$

Since \mathbb{V} and \mathbb{C} are known by singular value decomposition, we now try to find the transformation matrix \mathbb{T}^{-1} which provides physically meaningful values for \mathbb{S} and $\mathbb{X}(t)$, namely, positive absorption coefficients of the O and C forms and mole fractions varying in the range $[0, 1]$.

The matrix \mathbb{T}^{-1} transforms the eigenvectors \mathbb{V} into the spectra of the O and C forms. \mathbb{T}^{-1} can be written as $\begin{pmatrix} O_1 & C_1 \\ O_2 & C_2 \end{pmatrix}$, where (O_1, O_2) and (C_1, C_2) are the coefficients which multiply the two most important eigenvectors e_1 and e_2 to yield the spectra of the O and C forms, respectively. (O_1, O_2) are known experimentally and can be obtained by the scalar product of the UV-Vis absorption spectrum of the O form and each eigenvector, i.e. $O_i = e_i \cdot \varepsilon_O$, with $i = 1, 2$. However, (C_1, C_2) remain unknown because the C form can not be isolated. At any irradiation time t , one can write the equation

$$\underbrace{\begin{pmatrix} O_1 & C_1 \\ O_2 & C_2 \end{pmatrix}}_{\mathbb{T}^{-1}} \times \underbrace{\begin{pmatrix} \chi(t) \\ 1 - \chi(t) \end{pmatrix}}_{\mathbb{X}(t)} = \underbrace{\begin{pmatrix} c_1(t) \\ c_2(t) \end{pmatrix}}_{\mathbb{C}(t)} \quad (\text{SI.10})$$

where $(c_1(t), c_2(t))$ are obtained by singular value decomposition of the irradiation series. The system of Equations SI.10 has three unknowns (C_1 , C_2 and $\chi(t)$) and has no unique solution. But since the ratio of C_1 and C_2 must be constant in the full set of data, one can introduce the parameter $\kappa = \frac{C_1}{C_2}$ and solve the system of Equations SI.10 for different values of κ and all irradiation times. κ can be varied in a small range, where it provides physically meaningful results. Irradiation series with different excitation wavelengths further help to narrow down the possible values of κ and thereby determine the UV–Vis spectrum of the C form. This approach is illustrated next.

Uncertainty in the Composition of the Photostationary State

The sample was irradiated with quasi-monochromatic light emitted by an optical parametric amplifier (TOPAS-Prime, Light Conversion). The system delivers about 100 fs pulses with 4 kHz repetition rate. The sample was kept in a fused-silica cuvette and the beam was expanded with a negative lens, so that illumination was homogeneous over the full window. The average intensities employed ranged from 5 to 20 mW cm⁻², depending on the irradiation wavelength. The stationary absorption spectrum of the irradiated sample was typically measured every 5 s far from the photostationary state and every 20 s at the stationary state.

Irradiation of the O form with 285 nm light shifts the ground-state equilibrium towards the C form, see Figure SI 6. The spectrum evolves until the photostationary state is reached. At this point, irradiation with 570 nm light completely shifts the equilibrium back to the O form.

The absorption spectra in Figure SI 6 show clear isosbestic points at 285, 304 and 358 nm. It

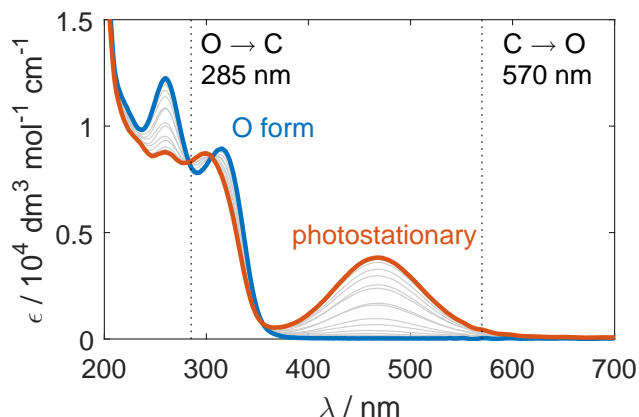


Figure SI 6: Ground-state UV–Vis absorption spectra of PSIV in methanol obtained after different irradiation times at the indicated wavelengths. The O form (blue) is irradiated at 285 nm. In turn, the photostationary state is irradiated at 570 nm and is thereby fully converted back to the O form.

is therefore possible to explain every spectrum in the series as a linear superposition of only two orthogonal components. The latter are found by singular value decomposition and are shown in Figure SI 7 together with their associated eigenvalues. The third component is also shown but its eigenvalue is so small that its contribution to the fit can be neglected.

The two first eigenvectors in Figure SI 7 are used as orthogonal basis set to fit the absorption spectra in the series. Obviously, any linear combination of the two eigenvectors is equally valid to fit the spectra at any irradiation time. In particular, we choose a linear combination where one of the vectors matches the spectrum of the O form and the other component of the basis set is defined by the κ parameter, which is the ratio between the coefficients of the first and second eigenvectors. κ can actually take any value but only the range between -1.5 and -6 produces physically meaningful results: positive UV–Vis absorption spectrum of the C form, see Figure SI 8, and positive mole fraction of the O form for any irradiation time, see Figure SI 9.

Figure SI 9 illustrates how big the uncertainty in the spectrum of the C form is. Any κ value between -1.5 and -6 is equally valid. However, the higher limit predicts a PS state where the O and

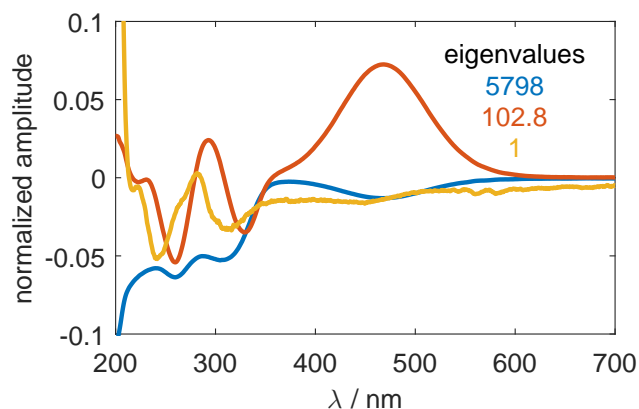


Figure SI 7: Eigenvectors resulting from the singular value decomposition of the irradiation series shown in Figure SI 6. Their associated eigenvalues are shown in the legend with corresponding colors.

C forms are in approximately equal amounts ($\chi \approx 0.55$). On the other hand, the lower limit of κ 's leads to a PS state where the equilibrium would be completely shifted towards the C form. Any situation in between yields an equally good description of the experiment.

We narrow down the range of possible values of κ in the next section. The composition of the PS spectra obtained by irradiation at several wavelengths is used to impose strong conditions in the spectral shape of the C form, so that the latter can be determined unambiguously.

Unambiguous Determination of the UV–Vis Absorption Spectrum of the C form

The irradiation experiments described in the previous section were conducted at 285, 304 and 357 nm, where the isosbestic points are located. They were further conducted at 330 nm and 570 nm. Irradiation at the latter wavelength completely shifts the equilibrium towards the O form.

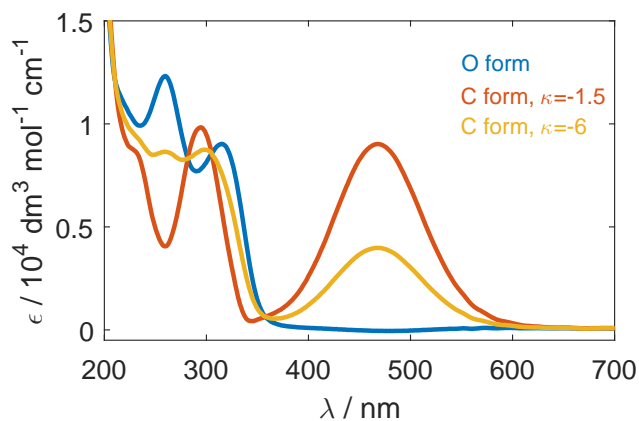


Figure SI 8: UV-Vis Absorption spectra measured for the O form (blue). The spectra of the C form can not be determined unambiguously. A κ value of -1.5 leads to the spectrum shown in red for the C form. In turn, $\kappa = -6$ leads to the yellow spectrum.

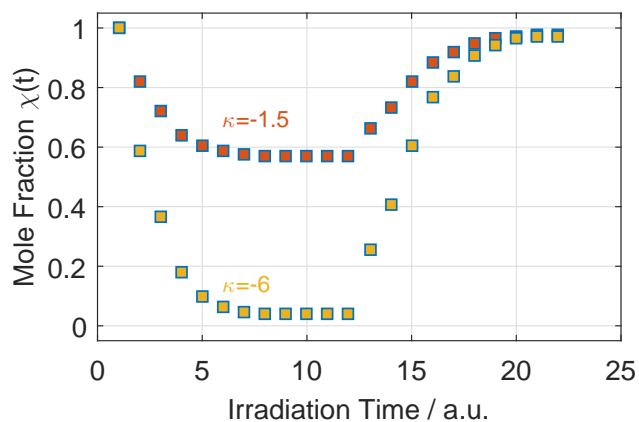


Figure SI 9: Mole fractions deduced for the O form in the irradiation experiment of Figure 6 if values of -1.5 (red) and -6 (yellow) are assumed for the parameter κ . The sample was irradiated at 285 nm up to irradiation time point number 12, when the PS state was achieved. Irradiation at 570 nm was started right afterwards, resulting in a shift of the ground-state equilibrium towards the O form.

Remarkably, the photostationary states resulting from irradiation at the isosbestic points are virtually equal (Figure SI 10), which by Equation SI.3 means that the quantum yield ratio for the $O \rightarrow C$ and $C \rightarrow O$ processes does not depend on excitation wavelength in the range between 285 and 357 nm. Therefore, any differences in the photostationary states obtained by irradiation within this range can be directly related to the absorption coefficients of the O and C forms at the excitation wavelength.

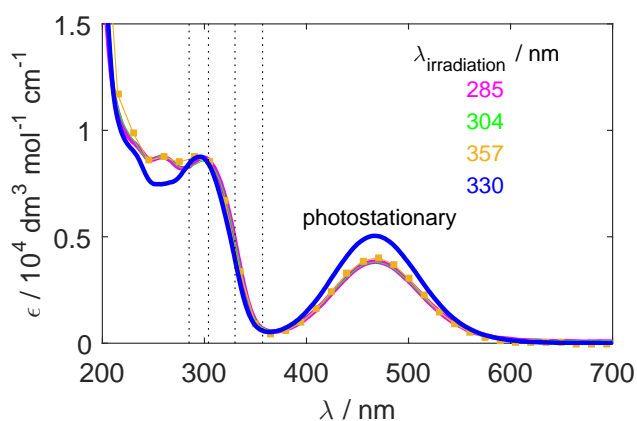


Figure SI 10: Absorption spectra of the photostationary states obtained by irradiation at the indicated wavelengths. Note that the spectra resulting from irradiation at the 285, 304 and 357 nm isosbestic points are virtually equal. On the contrary, the photostationary state at 330 nm is richer in the C form.

Figure SI 11 shows the UV–Vis absorption spectra obtained at various irradiation times for all excitation wavelengths used in this work: 285, 304, 330, 357 and 570 nm. All excitation wavelengths are indicated in Figure SI 11 by dotted vertical lines.

The data set in Figure SI 11 was analyzed. The respective eigenvectors and eigenvalues are shown in Figure SI 12. The two most important eigenvectors provide a very good description of the data. As explained above, they can now be combined to reproduce the spectrum of the O form and to predict physically meaningful mole fractions and C spectra. The latter are obtained for κ

values ranging from -1.6 to -6. Note that the negative sign in κ is related to the (arbitrary) negative amplitude of the first eigenvector. The so-deduced limiting values of the mole fractions are shown in Figure SI 12.

κ was then systematically varied between -6 and -1.6 until the spectra of the O and C forms lead to absorption coefficient ratios $\frac{\varepsilon_O^\lambda}{\varepsilon_C^\lambda}$ consistent first, with the PS concentrations deduced for 330 nm irradiation and second, with the $\frac{\Phi_{rc}^\lambda}{\Phi_{ro}^\lambda}$ ratio resulting from the irradiation at the isosbestic points. This self-consistent solution was obtained by inspection, although it could be easily integrated in a fitting procedure. The optimal value of the κ parameter is -2.273 and leads to the absorption coefficients of the O and C forms in Figure SI 14. It is further deduced that the ratio $\frac{\Phi_{rc}^\lambda}{\Phi_{ro}^\lambda}$ amounts to 1.44 while the ratio $\frac{\varepsilon_O^\lambda}{\varepsilon_C^\lambda}$ is 2.33 at 330 nm.

The so obtained UV–Vis spectra are in excellent agreement with those measured after separation of the O and C isomers by HPLC, Figure SI 15. Therefore, we conclude that about 40% of the molecules are in the O form in the PS states obtained upon irradiation at the isosbestic points found at 285, 304 and 357 nm. In contrast, the PS mole fraction of the O form decreases to about 20% upon irradiation at 330 nm, Figure SI 16. This is the minimum concentration of the O form achievable in the investigated spectral range.

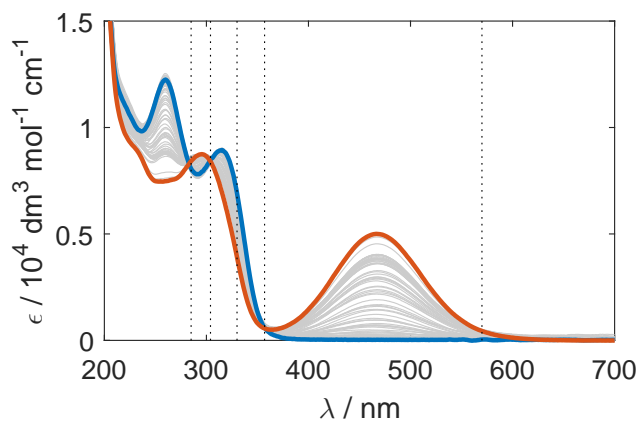


Figure SI 11: Absorption spectra of the the PS-IV photoswitch obtained by irradiation at 285, 304, 330, 357 and 570 nm. The irradiation wavelengths are indicated as vertical dotted lines. Blue and red spectra mark the photostationary states with highest O and C concentrations, respectively.

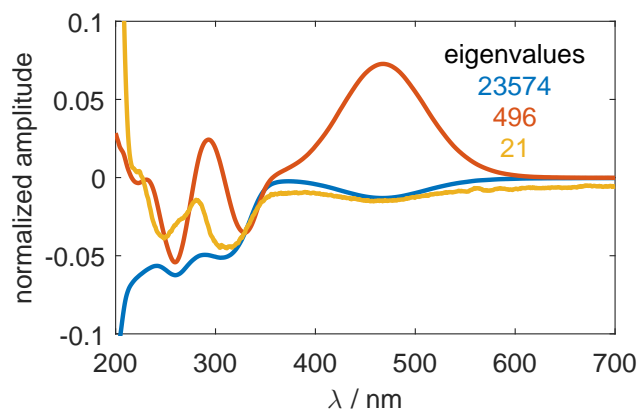


Figure SI 12: Eigenvectors and eigenvalues calculated for the spectral set shown in Figure SI 11. Eigenvectors and their associated eigenvalues are shown with corresponding colours.

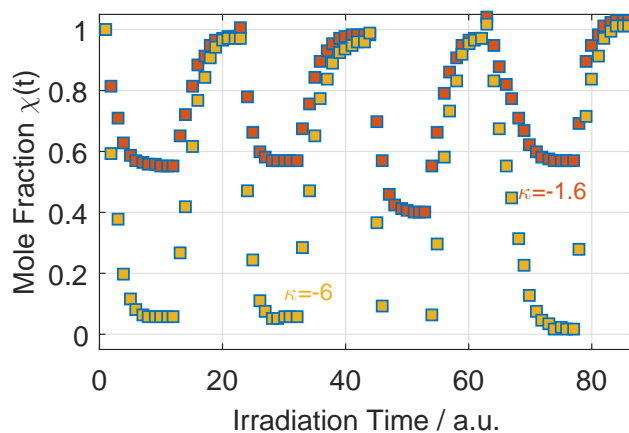


Figure SI 13: Mole fractions of the O form deduced for all the spectra in Figure SI 11 after assuming κ values of -1.6 (red) and -6 (orange). From left to right irradiation wavelengths of 285, 570, 304, 570, 330, 570, 357 and 570 nm are shown. Regions with zero slope correspond to photostationary states while discontinuities appear whenever the irradiation wavelength was changed. The data demonstrate robust photoswitching behaviour.

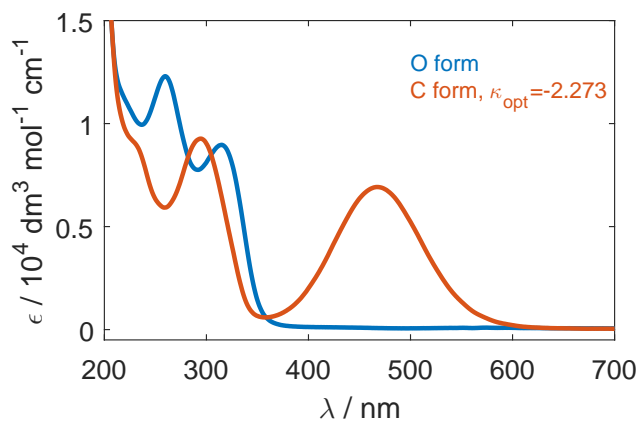


Figure SI 14: Absorption spectra of the O (blue) and C (red) forms deduced from the self-consistent analysis of the spectral series shown in Figure SI 11. The optimal value of the κ parameter, which defines the shape of the C spectrum, is also indicated.

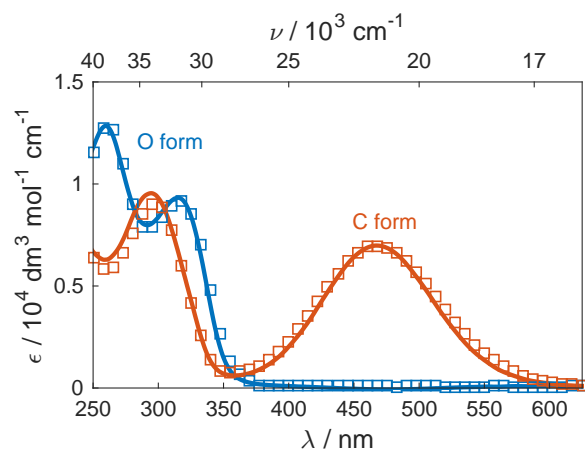


Figure SI 15: Absorption coefficients of the O (blue solid line) and C (red solid line) forms as obtained by the procedure outlined in this section. The corresponding scatter plots show the spectra of the pure isomers measured after separation by HPLC. Minor differences may be attributed to different experimental conditions (water/ ethanol mixture vs. pure methanol, different spectral composition of light in the various experiments).

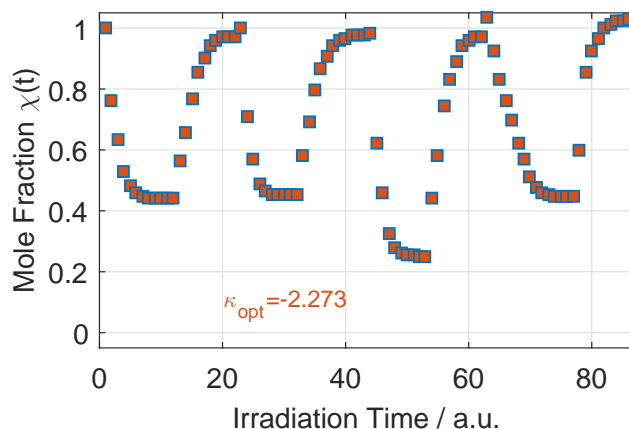


Figure SI 16: Mole fraction of the O form deduced for the spectra in Figure SI 11 for a κ value of -2.273. The latter leads to physically meaningful mole fractions and absorption coefficients consistent with the composition of the photostationary states obtained by irradiation at various wavelengths. From left to right, mole fractions for irradiation at 285, 304, 330 and 357 nm are shown (regions with negative slope). The photostationary state (regions with zero slope at $\chi < 1$) were driven back to the pure O form (zero slope with $\chi \approx 1$) by irradiation at 570 nm.

d) TA evolution in the 250 ps time scale

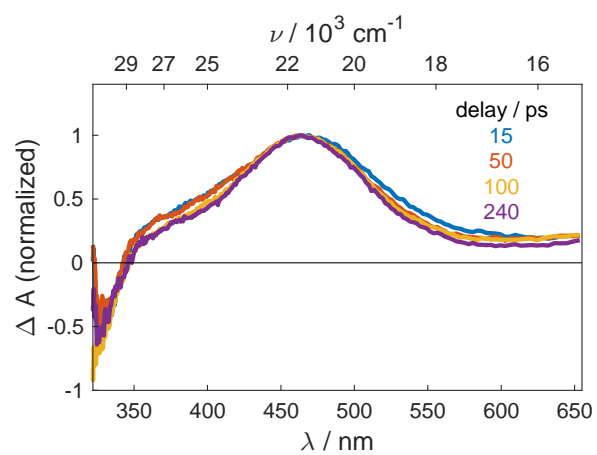


Figure SI 17: Time evolution of the transient absorption spectrum of PS-IV in the 200 ps time scale. Parallel pump-probe polarization is shown. Spectra were normalized at their maxima to better expose the soft blue shift and narrowing of the ESA band in this time scale.

e) Comparison of measurements performed with parallel and perpendicular polarizations

Parallel and perpendicular polarizations were measured independently and averaged. Typically, eight independent scans were averaged. Both kind of signals overlap from 200 ps delay onwards, meaning that the isotropic distribution of transition dipoles has been reached by this time, i.e. the ensemble of excited molecules is randomly oriented by 200 ps, see Figure SI 18. The signal for magic angle polarization was calculated with the formula $\Delta A_{magic} = (\Delta A_{\parallel} + 2\Delta A_{\perp}) / 3$.

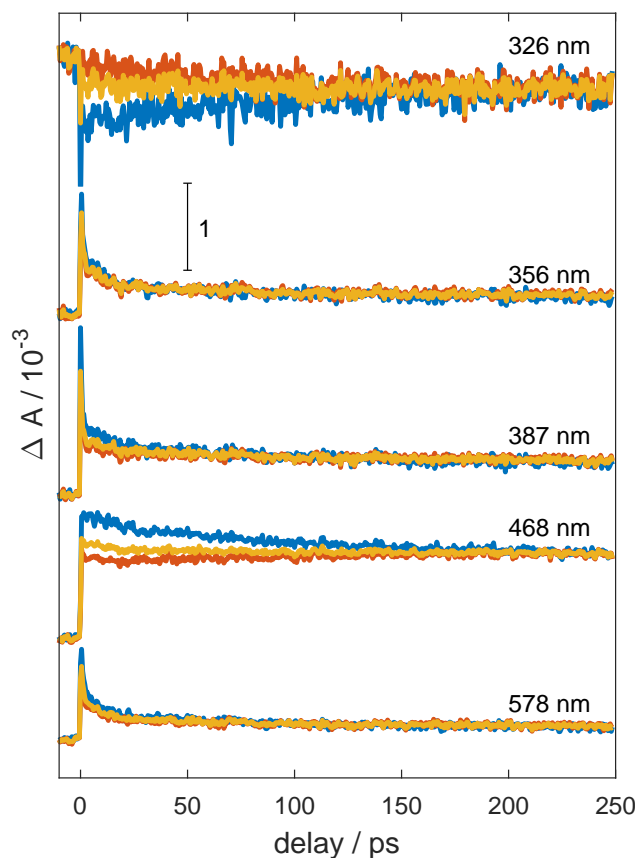


Figure SI 18: Transient absorption traces obtained for PS-IV in methanol at the indicated probe wavelengths. Measurements with parallel pump-probe polarization are shown in blue, while the orange traces show the measurements corresponding to the perpendicular polarization. Magic angle signals (dark yellow) are calculated from the measurements done with the experimentally determined traces for perpendicular and parallel polarizations.

f) Detailed Information about Global Fits in the 2 and 15 ps time windows

A summary of the results obtained in local multiexponential fits performed on transient absorption measurements with parallel polarization and in the 2 ps time scale (5 fs time steps) is shown in Figures SI 19 and SI 20. A monoexponential fit including a non-decaying component (Figure SI 19) provides good results. The time zero delays and the instrument response functions so obtained are consistent with our analysis of the coherent solvent signal (Figures SI 3 and 4). However, the decay time shows a strong spectral dependence. On the blue wing, the optimal decay time is about 0.3 ps at 350 nm. It becomes lower than 0.1 ps around 475 nm and increases to 0.5 ps on the red edge of the spectral window. This indicates that the signal evolution is not single exponential but at least biexponential. The results of this new fit are shown in Figure SI 20. One observes that the two decay times scatter around 0.1 and 0.5 ps. They are best defined in the red spectral wing and from 400 to 450 nm. Elsewhere, they are much more entangled because of their small amplitudes and poor signal-to-noise. A global fit shall yield more precise values of the decay times and their associated amplitudes. The fit quality is demonstrated in Figure 4 of the main text, while associated SADS are gathered in Figure 5.

A similar analysis was performed for the measurements in the 15 ps time scale. A new decay component appears and shows values scattering around 10 ps. The results of the corresponding global biexponential fit are shown in Figure SI 21.

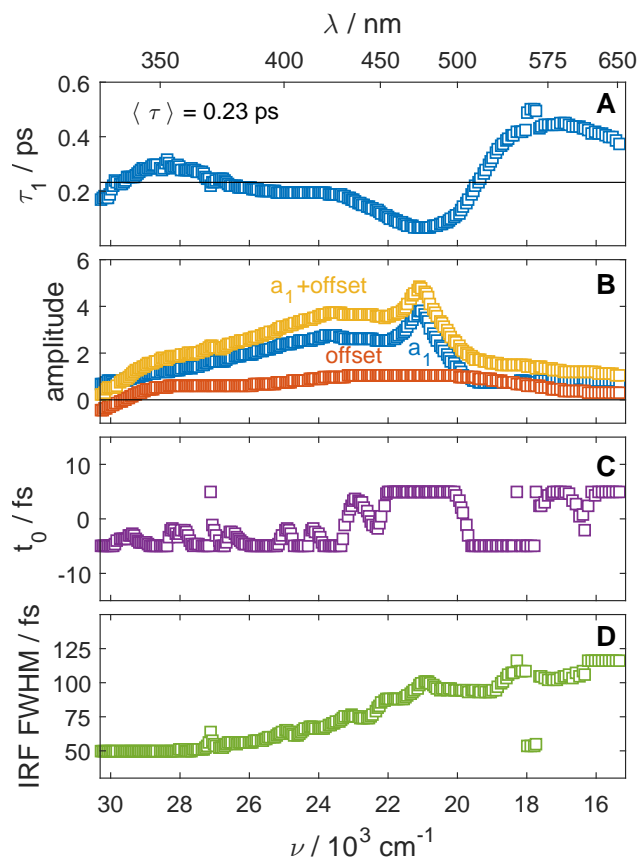


Figure SI 19: The transient signal measured for the first 2 ps delay and parallel polarization was fitted to a monoexponential and a step (offset) function for all the probe wavelengths. Both functions were convoluted with the instrument response function (IRF), which is assumed to be Gaussian. From top to bottom, panel **A** shows the fitted exponential decay time (blue) as function of the probe wavelength. The average lifetime is indicated in the inset. The associated amplitude is shown in panel **B** (a_1 , blue) together with the offset amplitude (orange). The sum $a_1 + \text{offset}$ provides, in a simple one step kinetic model, the species associated difference spectrum of the decaying component (dark yellow). Fitted values of the time-zero position (t_0 , violet) and the FWHM of the IRF (green) are shown in the panels **C** and **D**, respectively.

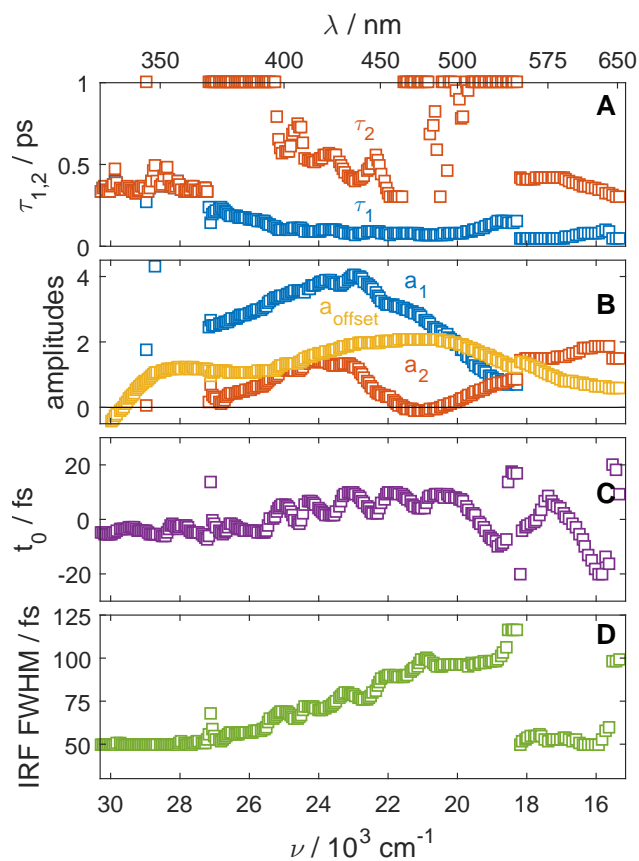


Figure SI 20: The transient signal measured for the first 2 ps delay and parallel polarization was fitted to a biexponential and a step (offset) function for all the probe wavelengths available. Both functions were convoluted with the instrument response function (IRF), which is assumed to be Gaussian. Panel **A** shows the fitted exponential decay times (blue and red squares) as function of the probe wavelength. Their associated amplitudes is shown panel **B** (a_1 and a_2 , blue and orange respectively) together with the offset amplitude (dark yellow). Fitted values of the time-zero position (t_0 , violet) and the FWHM of the IRF (green) are shown in Panels **C** and **D**, respectively.

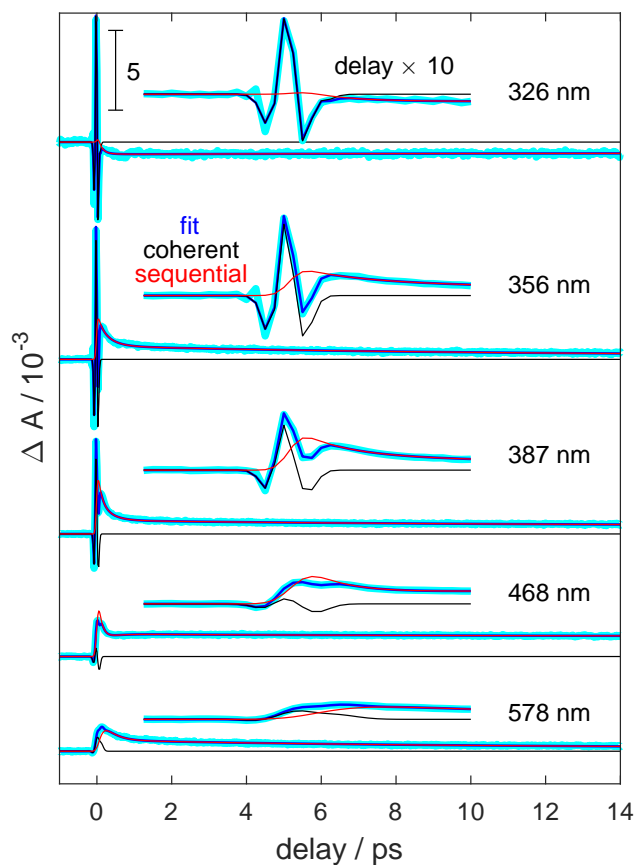


Figure SI 21: Biexponential free fit (dark blue) of the transient absorption signal (cyan) at the indicated probe wavelengths in the 15 ps timescale. The fitted function contains a set of basis functions that describe the coherent contribution at early time (black). The latter is in very good agreement with independent measurements of the non-resonant coherent solvent signal (see Figure 4 in the main text). The sequential contribution of the PS-IV molecule is extracted (red). The signal amplitude is given by the internal gauge. In the inset the same data are magnified by a factor of ten in the region around time zero for each wavelength. The amplitude was scaled by 0.8 in the data zoomed out for presentation purposes.

g) Calculation of the SADS from the DADS for a consecutive reaction model involving four species

The sequential part of the TA signal, $S(\lambda, t)$, can be explained as a sum of four basis functions: three exponentials $\exp[-(t - t_0)/\tau_i]$ (with $i = 1 - 3$) and a non decaying component, which is a Heaviside function $\mathcal{H}(t - t_0)$. All four basis functions are convoluted with the instrument response function. The last step is however omitted and t_0 is assumed to be exactly zero for the sake of clearness. Therefore, the signal at pump-probe time delay t and for the probe wavelength λ is given by:

$$S(t, \lambda) = \sum_{i=1}^3 a_i(\lambda) \exp(-t/\tau_i) + a_o \cdot \mathcal{H}(t - t_0) \quad (\text{SI.11})$$

The signal can be easily expressed in matrix form. One defines the matrix \mathbb{S} which contains the TA signal as function of probe wavelength and delay time. \mathbb{S} has dimensions $n_\lambda \times n_t$, being n_λ and n_t the number of probe wavelengths and the number of delay times measured in the experiment, respectively. The matrix \mathbb{A} contains the amplitudes $a_i(\lambda)$ of the basis functions in columns and has dimensions $n_\lambda \times n_c$, where n_c is the number of basis functions in the fitting function, four in the present case. Finally, the matrix $\mathbb{B}(t)$ contains the basis functions in rows and has dimensions $n_c \times n_t$. The matrix form of Equation SI.11 is

$$\underset{(n_\lambda \times n_t)}{\mathbb{S}} = \underset{(n_\lambda \times n_c)}{\mathbb{A}} \cdot \underset{(n_c \times n_t)}{\mathbb{B}} \quad (\text{SI.12})$$

Alternatively, the signal can also be explained as a sum of the time-dependent concentrations $c(t)$ multiplied by the absorption cross-sections (σ) of all intervening species. Thus, the multiplication of the matrices $\mathbb{\Sigma}$ and $\mathbb{C}(t)$, which contain the absorption cross-sections in columns and the time dependent concentrations in rows, respectively, explains the signal as good as the multiexponential fit Equation SI.12, if the kinetic model is correct. Therefore, the equality $\mathbb{A} \cdot \mathbb{B} = \mathbb{\Sigma} \cdot \mathbb{C}$ holds.

The time-dependent concentrations are sums of exponential functions for kinetic models involving first and pseudo-first order reaction stages only. The coefficients multiplying the exponential functions in the time-dependent concentrations are ratios between the rate constants and analytical expressions can be easily derived from the kinetic model. Hence, it is generally possible to express the time-dependent concentrations matrix \mathbb{C} as a product of a $(n_b \times n_b)$ coefficients matrix \mathbb{K} times the basis functions matrix \mathbb{B} .

$$\mathbb{S} = \Sigma \cdot \mathbb{K} \cdot \mathbb{B} \quad (\text{SI.13})$$

Therefore, it is deduced that the matrix of the exponential amplitudes \mathbb{A} is related to the absorption cross-sections matrix Σ by $\mathbb{A} = \Sigma \cdot \mathbb{K}$. The latter equality is obtained by comparing Equations SI.12 and SI.13.

The procedure here applied involves the multiexponential fit of the TA signal from which the amplitudes \mathbb{A} and a set of rate constants $\{k_i\}$ are obtained. The kinetic model provides the coefficients matrix \mathbb{K} with which the absorption cross-sections are calculated:

$$\Sigma = \mathbb{A} \cdot \mathbb{K}^{-1} \quad (\text{SI.14})$$

Since $\mathbb{K}^{-1} \cdot \mathbb{K} = \mathbb{I}$, being \mathbb{I} the identity matrix, the description of \mathbb{S} by the basis functions in the multiexponential fit is exactly as good as that obtained with the time-dependent concentrations and associated absorption cross-sections. For a consecutive model with four species and three rate constants, $\sigma_1 \xrightarrow{k_1} \sigma_2 \xrightarrow{k_2} \sigma_3 \xrightarrow{k_3} \sigma_4$, the \mathbb{K} matrix reads:

$$\mathbb{K} = \begin{bmatrix} 1 & 0 & 0 & 0 \\ -\frac{k_1}{k_1-k_2} & \frac{k_1}{k_1-k_2} & 0 & 0 \\ \frac{k_1 k_2}{(k_1-k_2)(k_1-k_3)} & -\frac{k_1 k_2}{(k_1-k_2)(k_2-k_3)} & \frac{k_1 k_2}{(k_1-k_3)(k_2-k_3)} & 0 \\ -\frac{k_2 k_3}{(k_1-k_2)(k_1-k_3)} & \frac{k_1 k_3}{(k_1-k_2)(k_2-k_3)} & \frac{k_1 k_2}{(k_1-k_3)(k_2-k_3)} & 1 \end{bmatrix} \quad (\text{SI.15})$$

It is assumed that only the state σ_1 is populated at earliest time. The concentrations were normalized to the initial concentration of the state σ_1 .

h) Spectral changes induced by excitation with higher photon energy

We close the Supporting Information with Figures SI 22 and SI 23 where intensity- and excitation-energy-dependence of the transient absorption signal are analyzed qualitatively. One observes an additional component in the transient absorption signal, which is most clear at delays earlier than 50 ps, see Figure SI 22. The spectral shape remains constant and independent of pump intensity at later delays. However, the transient absorption signal is seen to increase more than linearly upon increasing the pump intensity, which is interpreted as a contribution to the ring closing reaction by multiphoton excitation. Figure SI 23 compares the spectra obtained around 200 ps delay at different excitation wavelengths: 327 and 280 nm. All other experimental parameters are the same, especially the pump energy which was kept at 220 nJ. Excitation with higher excess of energy leads to a larger contribution of the non-productive long living component, demonstrating that the branching process proposed in Scheme 2 must occur before thermalization. One also notes that the long-living component can not be assigned to the parallel conformer of the O form because in that case no excitation energy dependence could be expected.

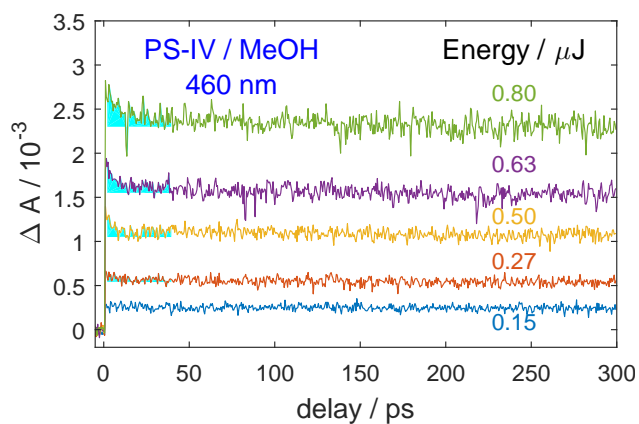


Figure SI 22: Transient absorption signal obtained at 460 nm upon 327 nm excitation at the indicated pump energies. Measurements were done with magic angle pump-probe polarization. An additional contribution is observed at early time for high pump energies (cyan shaded area).

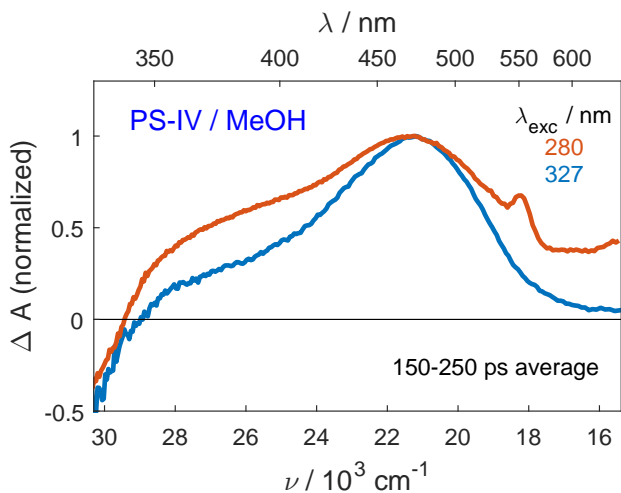


Figure SI 23: Transient absorption spectra averaged between 150 and 250 ps delay for 327 (blue) and 280 nm (orange) excitation. The spectra were normalized at their maxima.

References

- (1) Jiang, M.; Paul, N.; Bieniek, N.; Backup, T.; Hampp, N.; Motzkus, M. "Photocleavage of Coumarin Dimers Studied by Femtosecond UV Transient Absorption Spectroscopy". *Phys. Chem. Chem. Phys.* **2017**, *19*, 4597–4606.
- (2) Riedle, E.; Beutter, M.; Lochbrunner, S.; Piel, J.; Schenkl, S.; Sporlein, S.; Zinth, W. "Generation of 10 to 50 fs Pulses Tunable Through all of the Visible and the NIR". *Appl. Phys. B* **2000**, *71*, 457–465.
- (3) Möhring, J.; Backup, T.; Motzkus, M. "Shaper-Assisted Full-Phase Characterization of UV Pulses without a Spectrometer". *Opt. Lett.* **2010**, *35*, 3916–3918.
- (4) Kovalenko, S. A.; Dobryakov, A. L.; Ruthmann, J.; Ernsting, N. P. "femtosecond Spectroscopy of Condensed Phases with Chirped Supercontinuum Probing". *Phys. Rev. A* **1999**, *59*, 2369–2384.
- (5) Irie, M.; Mohri, M. "Thermally Irreversible Photochromic Systems. Reversible Photocyclization of Diarylethene Derivatives". *J. Org. Chem.* **1988**, *53*, 803–808.
- (6) Jong, J.; Lucas, L.; Hania, R.; Pugzlys, A.; Kellogg, R.; Feringa, B. L.; Duppen, K.; Esch, J. Photochromic Properties of Perhydro- and Perfluorodithienylcyclopentene Molecular Switches. *Eur. J. Org. Chem.* **2003**, *2003*, 1887–1893.